Microporous and Mesoporous Materials 258 (2018) 228–235

Contents lists available at ScienceDirect

Microporous and Mesoporous Materials

journal homepage: www.elsevier.com/locate/micromeso

Synthesis and structure of analcime and analcime-zirconia composite derived from coal fly ash cenospheres

Tatiana A. Vereshchagina [a, *], Ekaterina A. Kutikhina [a], Leonid A. Solovyov [a], Sergei N. Vereshchagin [a], Elena V. Mazurova [a], Yana Yu. Chernykh [a], Alexander G. Anshits [a, b]

[a] Institute of Chemistry and Chemical Technology SB RAS, Federal Research Center "Krasnoyarsk Science Center SB RAS", 50/24 Akademgorodok, Krasnoyarsk, 660036, Russia
[b] Department of Chemistry, Siberian Federal University, Svobodny pr. 79, Krasnoyarsk, 660041, Russia

ARTICLE INFO

Article history:
Received 24 May 2017
Received in revised form
23 August 2017
Accepted 12 September 2017
Available online 18 September 2017

Keywords:
Analcime
Cenospheres
Zirconia
Hydrothermal synthesis

ABSTRACT

Cubic analcime and analcime-zirconia composite with the Si/Al ratio of 2.04 and 2.16, respectively, was synthesized by hydrothermal treatment of coal fly ash cenospheres (Si/Al = 2.7) at 150 °C. The scanning electron microscopy with energy dispersive spectroscopy (SEM-EDS), powder X-ray diffraction (PXRD), X-ray photoelectron spectroscopy (XPS), synchronous thermal analysis (STA) methods were used to study the morphology, composition and structure of the products. Two main types of analcime bearing particles were obtained, such as hollow microspheres with attached analcime icositetrahedra of 5–50 μm in size and individual analcime crystals of a narrow particle size distribution (D_m = 41 μm) with incorporated zirconia (4.8 wt% Zr). The high quality of the crystalline fractions allowed an accurate full-profile PXRD analysis of complete analcime crystal structure and composition including anisotropic displacement parameters of all atoms and H-positions of water molecules.

© 2017 Elsevier Inc. All rights reserved.

1. Introduction

Analcime (ANA) is a natural occurring zeolite with a tetragon-trioctahedron habit which has a typical unit cell composition of $Na_{16}[(AlO_2)_{16}(SiO_2)_{32}]\cdot 16H_2O$ with a Si/Al molar ratio of 1.8–2.8 [1,2]. For its synthetic analogs the Si/Al ratio varies in a more wide range (1.5–3.0) depending on the cation nature, Si and Al sources, and conditions of synthesis [3]. Analcime has a 3-dimensional system of non-intersecting channels with the pore openings of 2.6 Å composed of four-, six- and eight-membered oxygen rings. High symmetry icositetrahedral morphology of analcime crystals is attractive for designing novel materials of a regular polyhedron form [4–6].

Due to minimal pore entrances compared to other zeolites, analcime is useful in separation of light gas/hydrocarbon mixtures, e.g. H_2/C_3H_8, based on the molecular sieving effect [7]. Synthetic analcimes, pure and metal (Mn, Ti, V) modified in T-positions, are efficient in a heterogeneous catalysis, e. g. cyclohexene oxidation in a liquid phase [8], and an ion exchange for removal of heavy metals from wastewater [9]. Analcime is the object of some studies in relation to the problem of nuclear waste disposal [10–14]. This narrow-pore zeolite can be used in nuclear waste burial as a sorptive barrier for radioactive elements because of its ability to bind actinide cations (U^{4+}, Th^{4+}) by sorption irreversibly providing the reliable immobilization of toxic metals [10]. The similarity of framework topology of analcime and pollucite, $(Cs_{1-n},Na_n)(H_2O)_n[AlSi_2O_6]$ [2], is the basis of methods for incorporation of radioactive ^{137}Cs in ANA phases resulting in pollucite or pollucite-analcime solid solutions [11–14].

Numerous studies are concerned with transition metal modified (exchanged/impregnated) zeolites as precursors of aluminosilicate-based ceramics including electronic ceramics [15] and ceramic bodies for electromagnetic shielding [16]. Zr bearing zeolites are of particular interest because they can be converted to refractory zirconia-aluminosilicate ceramic materials [17] having a potential as a chemically stable radioactive waste form [18]. Two kinds of Zr bearing zeolite precursors can be considered, such as zeolites modified at an atomic level by Zr^{4+} incorporation in T-sites or

* Corresponding author.
E-mail addresses: tatiana_ver@mail.ru (T.A. Vereshchagina), ekaterina_kutikhina@mail.ru (E.A. Kutikhina), leosol@icct.ru (L.A. Solovyov), snv@icct.ru (S.N. Vereshchagin), len.mazurowa@yandex.ru (E.V. Mazurova), yaninachernyh@yandex.ru (Y.Yu. Chernykh), anshits@icct.ru (A.G. Anshits).

https://doi.org/10.1016/j.micromeso.2017.09.011
1387-1811/© 2017 Elsevier Inc. All rights reserved.

cation positions, and zeolite based composites with Zr bearing matter embedded in the zeolite body. As for the analcime based precursor, the incorporation of large Zr atoms (R = 0,72 Å) in the dense analcime lattice and extra-framework positions is hardly probable due to the restrictions of bond lengths [1]. The Zr incorporation in the analcime body as a Zr bearing matter has not been reported yet.

Traditionally hydrothermal methods are applied to synthesize zeolites of different topologies starting from alkaline solution of pure chemicals (e.g. sodium silicate, sodium aluminate) [19]. As it was reported by Fang et al. [5], the lower rate of glass dissolution compared to that of gel or fine chemicals provides large analcime crystallites of up to 600 μm by hydrothermal treatment of sodium aluminosilicate glass at 150–210 °C.

The cost-effective synthetic routes to analcime are based on conversion of available natural and technogenic raw materials, such as clay minerals (Si/Al = 1.4) [8], coal fly ash (Si/Al = 1.6) [20], natural clinker (Si/Al = 2.5–3.0) [21], quartz syenite (Si/Al = 3.7) [22], and volcanic glass perlite (Si/Al = 4.6) [23]. However, most of the sources didn't provide a high purity of the analcime product containing the additional zeolite phases (GIS, CAN, FAU, etc.).

Recently, coal fly ash cenospheres (CFAC) were considered for synthesis of low-siliceous zeolites without seeding and templating as an alternative aluminosilicate source of the sphere shaped morphology and glassy structure with the appropriate silica-alumina composition (Si/Al = 1.1–2.9) [24–26]. The CFAC properties have been found to be suitable for their use as a template core and a Si and Al source in the zeolite synthesis. The advantage of this approach is possibility to use CFAC of required chemical and phase composition provided by separation of a CFAC concentrate on the basis of differences of individual globules in size, density, and magnetic properties [27–29]. In most cases the direct transformation of the CFAC material, in dependence on reaction parameters (temperature, duration, alkaline concentration, solid-to-liquid ratio), results in zeolitic phases of different structural types, such as NaX (FAU, JCPDS 12–0228), NaA (LTA, JCPDS 43–0142), NaP1 (GIS, JCPDS 40–1464), chabazite (CHA, JCPDS 12–0194), analcime (ANA, JCPDS 19–1180), and/or hydroxysodalite (JCPDS 11–401) [25]. Among them, only zeolite NaP1 was shown to crystallize as an individual phase under certain conditions (T = 100–120 °C, 1.5–2.5 M NaOH) [25,26]. As it has been noted by Vereshchagin et al. [25], analcime crystallized at elevated temperatures (T > 150 °C) but detailed results on zeolite formation from CFAC under temperatures higher than 120 °C were not reported anywhere.

In this paper, we report the hydrothermal synthesis of analcime and zirconia bearing analcime at 150 °C starting from CFAC with Si/Al = 2.7, characterization of their structure, composition and morphology by PXRD, SEM-EDS, XPS and STA.

2. Experimental

2.1. Chemicals and materials

Chemicals used in this work were of reagent grade quality obtained from the commercial supplier (OOO "Reactiv", Russia) and used without further purification.

The CFAC material used for the analcime synthesis was fraction −180 + 80 μm having a bulk weight of 0.38 g cm^{-3} and a specific surface area of 0.2 m^2 g^{-1} which was provided by the separation procedure of a CFAC concentrate resulted from combustion of Kuznetsk coal (Russia) at Tom-Usinskaya power plant (Kemerovo region, Russia) as it was reported earlier [27]. Chemical and mineral compositions of the initial CFAC material are summarized in Table 1. A total overview of the CFAC globules is shown in Fig. 1.

2.2. Synthetic procedures

Analcime was synthesized by hydrothermal treatment of a reaction mixture comprising of 10 g CFAC and 133 mL 1.5 M NaOH with 1.0 SiO_2/0.18 Al_2O_3/0.89 Na_2O/65 H_2O molar composition and liquid-to-solid (L/S) ratio of 5/1 (v/v). The reaction mixture was crystallized in a Teflon-lined stainless steel autoclave at 150 °C for 68 h under stirring by rotation of the autoclave (30 rpm). The grey solid phase (GS) was then washed several times with distilled water, filtered and dried at 65 °C for 24 h. The output of the solid calculated relative to the mass of initial CFAC was 81%. The subsequent separation of the GS product by particle sizes was done using sieves with apertures of 36 μm, 71 μm, 100 μm and 224 μm. Samples GS > 224 μm, GS 100–224 μm, GS 71–100 μm, GS 36–71 μm and GS < 36 μm were isolated by sieving the GS product with yields of 1.4, 49.0, 18.9, 28.5 and 2.2%, respectively.

Zirconia bearing analcime was synthesized by hydrothermal treatment of CFAC in sodium alkaline solution in the presence of zirconium (IV) citrate ammonium complex used as a Zr source. In a typical synthesis, 5 g zirconium (IV) citrate ammonium complex was added to 133 mL 1.5 M NaOH solution upon stirring at room temperature followed by addition of 10 g CFAC resulting in the reaction mixture of 1.0 SiO_2/0.18 Al_2O_3/0.89 Na_2O/0.15 ZrO_2/65 H_2O molar composition with L/S ratio of 5/1 (v/v). The mixture was transferred into the Teflon-lined stainless steel autoclave for crystallization by heating the suspension at 150 °C for 48 h under stirring by rotation of the autoclave (30 rpm). The white-and-grey solid (Zr-WGS) product was separated by filtration, washed with distilled water several times until neutral reaction of a supernatant occurred followed by centrifuging the suspension. Two layers were visually identified in centrifuge test tubes as white (Zr-WS) and grey (Zr-GS) solids, each of which was recovered and then dried at 65 °C for 24 h. The outputs of the Zr-WS and Zr-GS solids calculated relatively the mass of initial CFAC was 32 and 10%, accordingly. Each layer was additionally separated into fractions by particle sizes using sieves with apertures of 36 μm and 71 μm resulting in samples Zr-WS <36 μm, Zr-WS 36–71 μm with yields of 29 and 71%, respectively, and Zr-GS >71 μm, Zr-GS <36 μm with yields of 97 and 3%, respectively.

2.3. Characterization techniques

Chemical composition of CFAC fraction was determined according to State Standard (GOST) No. 5382-91 [30].

Powder X-ray diffraction data were collected on a PANalytical X'Pert PRO (Netherlands) diffractometer equipped with a solid state detector PIXcel using Cu Kα radiation over the 2θ range 12–120°. The samples were prepared by grinding with octane in an agate mortar and packed into a flat sample holder for the PXRD measurements in the Bragg-Brentano geometry. The full-profile crystal structure analysis was done using the Rietveld method [31] with the derivative difference minimization (DDM) [32] refinement.

Morphologies of product particles were identified by scanning electron microscopy (SEM) using TM-1000 and TM-3000 (Hitachi, Japan) instruments. To study elemental composition of surfaces and polished sections of analcime particles the SEM-EDS examination was performed using the TM-3000 microscope equipped with the Bruker microanalysis system including an energy-dispersive X-ray spectrometer with a XFlash 430 H detector and QUANTAX 70 software. The polished sections of analcime particles were prepared by fixing in an epoxy resin with successive grinding and polishing with the use of STRUERS materials and equipment

Table 1
Chemical and mineral composition (wt%) of the initial CFAC material.

Elements in terms of oxides								Si/Al	Crystal phases			Glass phase
SiO_2	Al_2O_3	Fe_2O_3	Na_2O	CaO	MgO	K_2O	TiO_2		quartz	mullite	calcite	
67.6	21.0	3.0	0.9	2.2	1.8	2.8	0.2	2.7	3.4	0.8	0.5	95.4

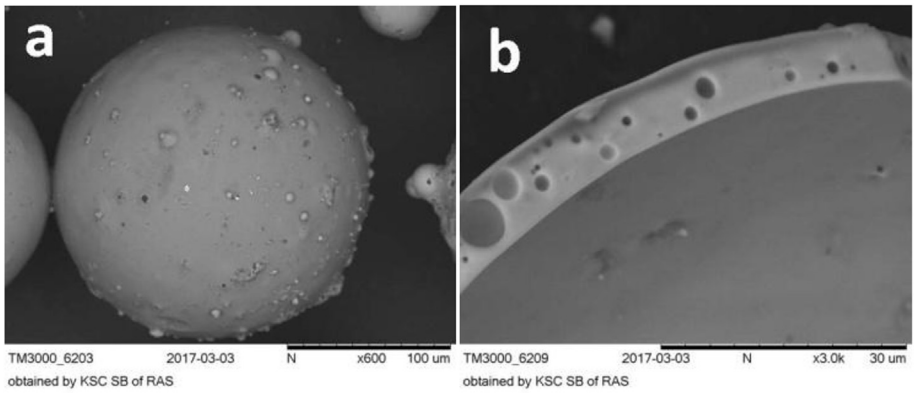

Fig. 1. SEM images of the initial CFAC material: (a) CFAC globule; (b) cross-section of the CFAC wall.

followed by the deposition of a platinum layer of ~20 nm thickness. Analysis was carried out at an accelerated voltage of 15 kV in a mapping mode. The data accumulation time was 10 min.

Thermal analysis was performed on a STA Jupiter 449C device (Netzsch, Germany) under a dynamic argon-oxygen atmosphere (20% O_2, 50 mL/min total flow rate). Platinum crucible with perforated lids was used and the sample mass taken for the measurement was 16.6 mg. The measurement procedure consisted of a temperature stabilization segment (30 min at 40 °C) and a dynamic segment at a heating rate of 10°/min.

The particle size distribution was determined by measuring the average diameter of particles with the use of "Msphere" software as it was reported earlier [29]. Digital images were obtained in reflected and transmitted light on a Carl Zeiss Axioskop 40 (Germany) optical microscope equipped with a Zeiss W–PI 10x/23 eyepiece and a Canon PowerShot A640 digital camera. The diameter was determined for each globule from the digital images processed with "Msphere" software. Statistical data on particle's diameters were obtained based on the analysis of 5364 images.

Chemical composition and element states were determined by X-ray photoelectron spectroscopy using a spectrometer SPECS (Germany) equipped with a PHOIBOS 150 MCD9 electron energy analyzer when exciting X-ray tube by Mg K_α radiation. The analyzer transmission energy was 20 eV for summarizing spectra and 8 eV for individual scans. Powdered samples were immobilized at a two-sided sticky carbon tape. Vacuum in an analytical chamber was not worse than $1 \cdot 10^{-9}$ mbar. Correction for the electrostatic recharging of samples was introduced taking into account the position of C1s line (binding energy is 285.0 eV) arising from the layer of hydrocarbon contaminations. To eliminate the recharging heterogeneity, treatment with low electrons was applied. Spectra were processed by SpecsLab and CasaXPS software. The reference material was ZrO_2 prepared according to Trens et al. [33].

3. Results and discussion

According to SEM data, solids produced as a result of the Zr free and Zr involving syntheses are differed by the particles morphology and size distribution as well as the degree of conversion of the CFAC material. Another peculiarity of the syntheses is the product outputs differing by two times. The low output in the Zr bearing reaction mixture can be a result of a colloid state of a considerable part of aluminosilicate which is hardly separated from a liquid phase.

The general feature of the syntheses is that zeolite analcime was the single zeolite phase identified in both products by PXRD. The detailed comparison of two analcime bearing products by their morphology, composition and structure are presented in later sections.

3.1. Morphology and composition of analcime particles

SEM images of typical particles occurred in different GS fractions of the Zr free synthesis product are shown in Fig. 2. The main types of particles entering the GS > 224 μm and GS 100–224 μm fractions are microsphere-like hollow globules and their fragments with partial icositetrahedral crystals of zeolite analcime [2] attached to external and internal surfaces (Fig. 2 a, b). The dimensions of the outside analcime crystals vary in a wide range - from 3 to 5 μm to 30–50 μm, the smaller analcime particles of 1–10 μm being located inside the broken microspheres. The content of the intact analcime bearing globules is considerably lower in the GS 71–100 μm and GS 36–71 μm fractions which include predominantly fragments of broken CFAC with attached analcime crystals, agglomerates of semi-crystals and twinned crystals (Fig. 2 c). The single analcime particles of less than 36 μm get together in the GS < 36 μm fraction (Fig. 2 d) but their content is rather small and does not exceed 2.2 wt%.

Thus, based on the SEM observation one can conclude that under conditions of synthesis the growth of analcime crystals takes place preferably at the CFAC surface.

The SEM-EDS of the analcime crystals gave an atomic ratio of about 1.1 Na/1.9 Si/1.0 Al within the range of the Si/Al ratio of the zeolite analcime [1].

As for the Zr involving synthesis, the SEM study of Zr-WS and Zr-GS products has shown that the Zr-WS product includes only particles of a tetragon-trioctahedron habit being typical of zeolite analcime crystals (Fig. 3 a, b) [2]. All the crystals can be

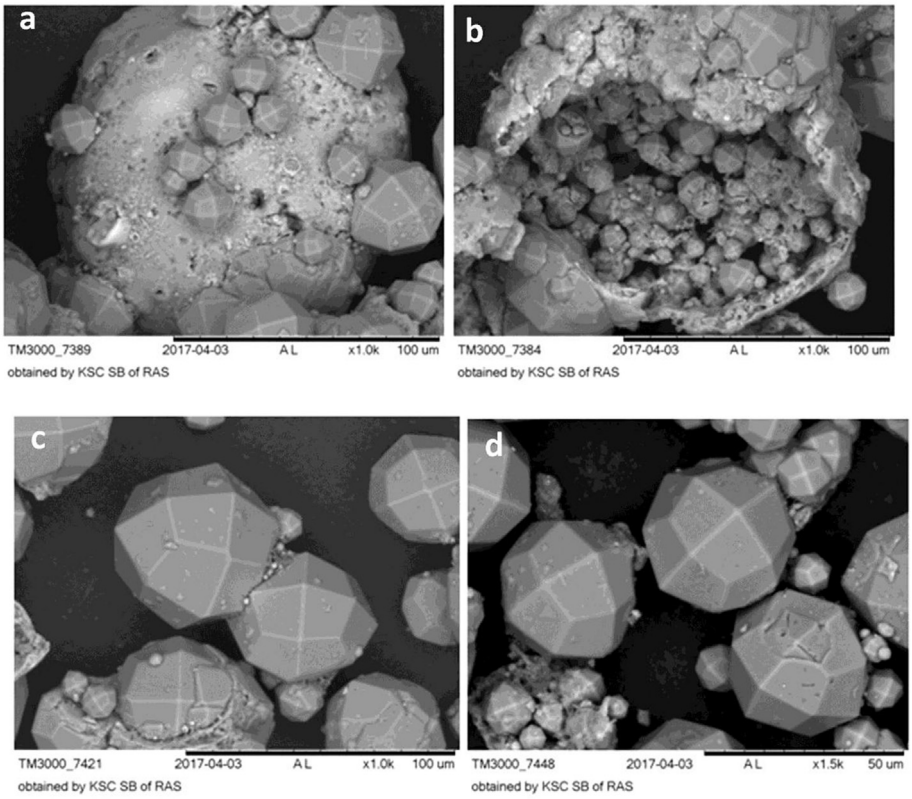

Fig. 2. SEM images of analcime bearing particles resulted from the Zr free synthesis: (a) analcime bearing globule; (b) broken microsphere filled with analcime particles; (c) twinned analcime crystal; (d) single analcime crystals.

characterized as icositetrahedra (211) with 24 identical facets of a cubic symmetry which belongs to the cubic *m3m* point group [34].

Analcime-bearing CFAC globules were revealed in the fraction Zr-GS >71 μm (Fig. 3 c) giving rise to analcime semi-icositetrahedra having an attached piece of the mother CFAC material in its base (Fig. 3 d). The halved analcime particles are concentrated in the fraction Zr-WS<36 μm and fractions Zr-GS (Zr-GS 36–71 μm; Zr-GS <36 μm), the later ones being enriched in partially dissolved CFAC glass fragments. It can be supposed that the presence of the halved analcime particles together with analcime crystals of a perfect intact morphology would be due to two routes of analcime formation, such as the crystal growth both in the reaction solution and on the CFAC surface. The hydrolyzed forms of zirconium salt occurring in the alkaline reaction mixture are likely to be the primary nuclei of crystallization.

As shown in Fig. 4, the intact analcime particles are characterized by the narrow size distribution with maximum at 41 μm. Analcime crystals with dimensions of 38–43 μm predominate in the Zr-WS product with their content of about 70% and are the main part of the fraction Zr-WS 36–71 μm. Particles measuring more than 71 μm were not found. The fraction Zr-WS<36 μm consists of 19–36 μm particles, among them both intact icositetrahedra and semi-icositetrahedra were detected. It can be proposed that formation of large analcime crystals of the narrow particle size distribution in the presence of hydrolyzed Zr forms are controlled by the ratio of two parameters, such as the release rate of silicate and aluminate species by dissolution of CFAC glass and the rate of crystal growth on the Zr species achieved under the reaction conditions.

The SEM-EDS of polished cross-sections of individual analcime particles gave an atomic ratio of about 1.0 Na/2.1 Si/1.0 Al which is close to that of the Zr free analcime. The presence of Zr matter inclusions in the bulk of the analcime crystals is supported by the SEM-EDS measurements of local concentrations of elements over analcime crystal cross-sections which are differed by the Zr content (Fig. 5a, Table 2, Fig. S1). Zirconium species are visible as contrast white spots on facets of analcime icositetrahedra, surfaces of all analcime bearing particles and in the bulk of crystals (Figs. 3 and 5). The average Zr content in the analcime particles was about 4.8 wt%.

According to the XPS data, the local charges of Zr atoms found in the analcime crystals (Zr-WS 36–71 μm) and Zr atoms being part of zirconia are close (Fig. 6) indicating that the most probable state of zirconium occurred in the Zr bearing analcime (Zr-ANA) is zirconia.

As shown in Fig. 7, the thermal conversion of Zr free analcime particles (GS 100–224 μm) includes two stages. The first broad endothermic DSC peak with the substantial mass loss is situated at 100–460 °C (T_m = 365 °C, total mass loss Δm = 8.06 wt%) and is accompanied by the parallel increase of intensity of m/z = 18 (H_2O) ion due to water elimination. An incomplete cenosphere-to-analcime transformation is a reason for a reduced mass loss compared to the theoretical water content of 8.17 wt%. The second exothermic peak is observed at 790–880 °C (T_m = 797 °C). The absence of mass change at this temperature interval suggests that the exo-effect is caused by the solid state transformation (re-crystallization) of analcime. A similar temperature interval of water elimination is observed for Zr-analcime (Zr-WS 36–71 μm), the Zr species inclusions in the analcime crystals can be a reason for a reduced mass loss (Δm = 7.87 wt%). There was no pronounced exothermic effect found at 797 °C but the PXRD analysis of Zr-analcime calcined at 900 °C revealed ZrO_2 and nepheline phases in the calcination product (Fig. S2) so the observed broad peak at

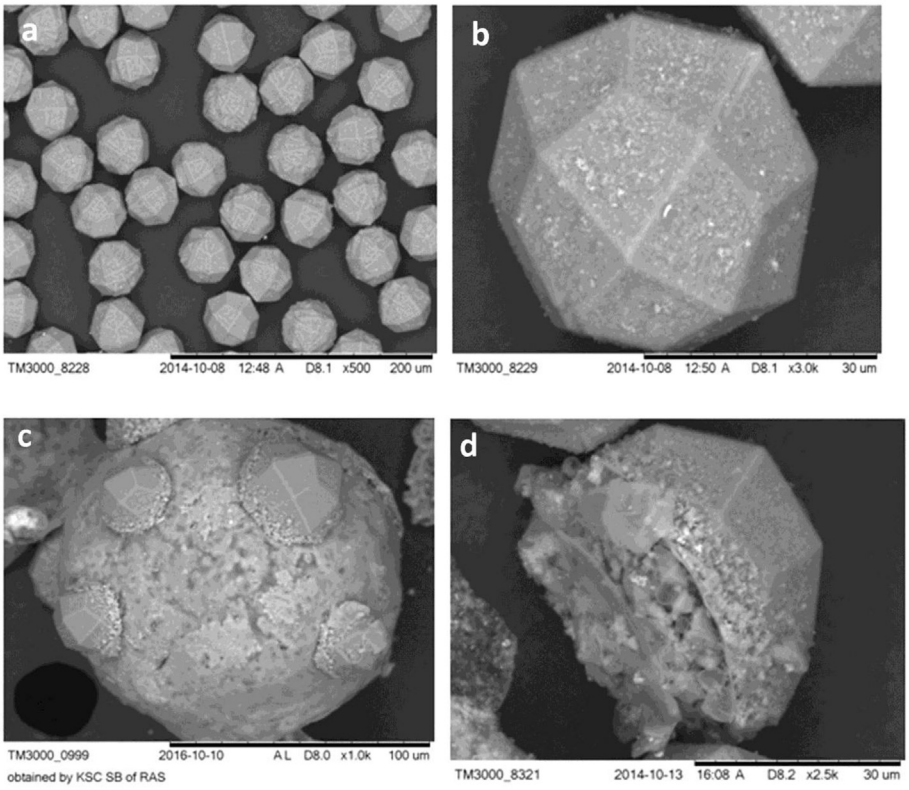

Fig. 3. SEM images of Zr-analcime and Zr-analcime bearing particles: (a, b) analcime icositetrahedra; (c) analcime-bearing microsphere particle; (d) semi-icositetrahedron grown on the CFAC surface.

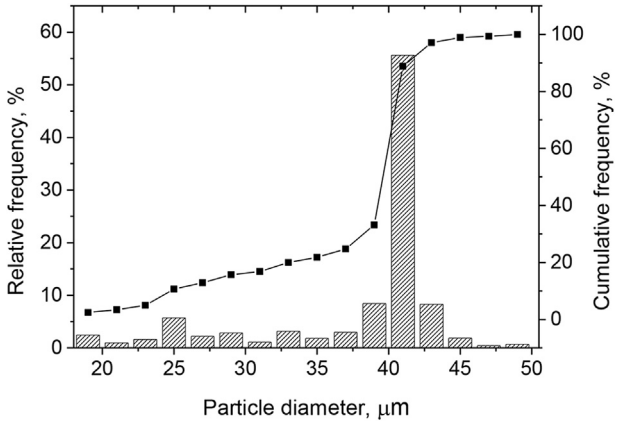

Fig. 4. Particle size distribution for analcime fraction Zr-WS.

about 800–840 °C can be also assigned to the Zr-analcime recrystallization.

3.2. Crystal structure of analcime and Zr-analcime

In order to assess the influence of Zr on the structural characteristics of analcime phase crystallized in its presence, a full-profile PXRD crystal structure analysis was carried out for both pristine and zirconia-incorporated analcime samples. It should be noted that detailed and reliable PXRD analysis of analcime crystal structure and composition presents a challenging task. The cations, vacant sites and water molecules in an approximately cubic crystal lattice of analcime are distributed statistically, giving rise to local symmetry variations and distortions (displacements) of atomic positions. Refinement of such crystal structures requires a complete model including the anisotropic displacement parameters of all

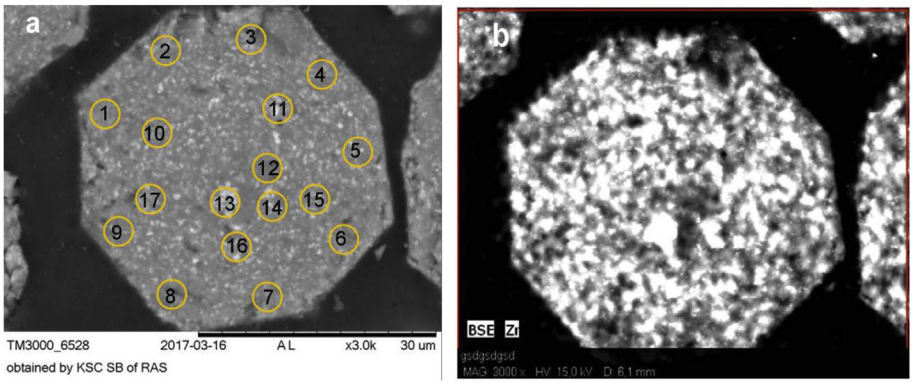

Fig. 5. SEM (a) and BSE (b) images of the Zr-analcime polished cross-section: (a) with designation of the analysis points; (b) Zr distribution map over cross-section of the crystal.

Table 2
Local elemental composition of Zr-analcime particles according to the SEM-EDS data.

No.*	Content, wt%				
	O	Si	Al	Na	Zr
1	49.0	25.0	11.7	11.4	2.9
2	47.7	24.3	11.8	10.4	5.8
3	47.9	26.6	11.0	10.1	4.4
4	46.9	26.7	12.5	9.5	4.4
5	46.3	26.2	12.4	10.0	5.1
6	44.2	26.8	13.3	9.5	6.2
7	50.4	24.0	11.8	10.0	3.8
8	47.6	26.8	13.1	10.4	2.1
9	50.8	23.8	11.5	11.1	2.8
10	48.5	25.1	11.6	9.9	4.9
11	47.9	25.9	11.7	9.4	5.1
12	49.3	26.0	12.5	9.3	2.9
13	46.2	25.4	10.9	9.4	8.1
14	47.3	26.8	11.2	9.1	5.6
15	47.5	27.2	11.0	9.2	5.1
16	46.7	26.4	11.2	9.5	6.2
17	49.1	26.4	10.8	9.1	4.6

* As in Fig. 5a.

atoms and precise H-positions related to water. The anisotropic parameters and some hydrogen-related positions for cubic analcime were derived in a single-crystal neutron diffraction study of a mineral analcime [35]. However, as the authors of [35] noted, the resulted H-positions were not realistic since none of the H-O-H and Na-O-H angles accorded reasonably with the normal geometry of the Na-coordinated water molecules. In the present study, complete crystal structures of the analcime samples were refined using the DDM method that has been proven to provide detailed and reliable structural information from powder diffraction data including the anisotropic displacement parameters and positions of H-atoms [36–38].

A comparison of observed and calculated PXRD patterns for both samples is presented in Fig. 8. The refined compositions, lattice parameters and experimental details are summarized in Table 3. The atomic coordinates, site occupancies and anisotropic displacement parameters are available in the crystallographic information files (CIFs) from the supplementary material.

An ellipsoid plot of analcime crystal structure refined by DDM is compared in Fig. 9 with that resulted from the single-crystal neutron diffraction [35]. As seen, the shapes of atomic

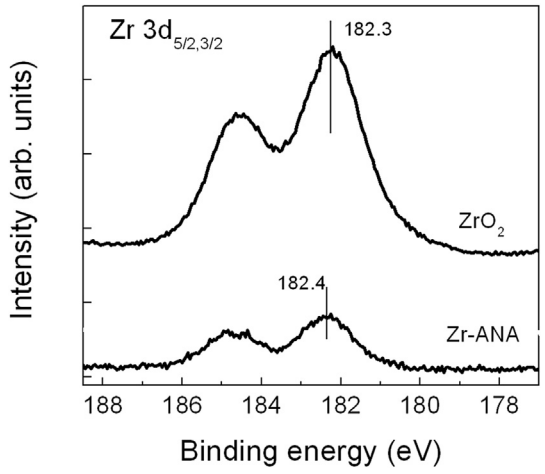

Fig. 6. XPS patterns of Zr 3D doublet in Zr-analcime and zirconia.

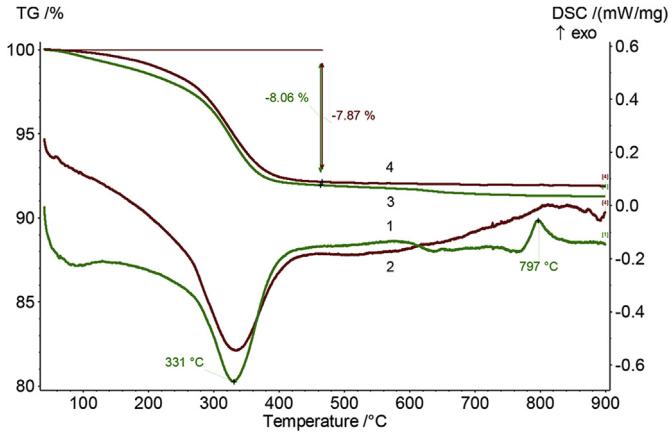

Fig. 7. DSC (1,2) and TG (3,4) curves of the thermal transformation of analcime particles (1,3) and Zr-analcime (2,4) in a dynamic argon-oxygen atmosphere 20% O_2-Ar, 10°/min.

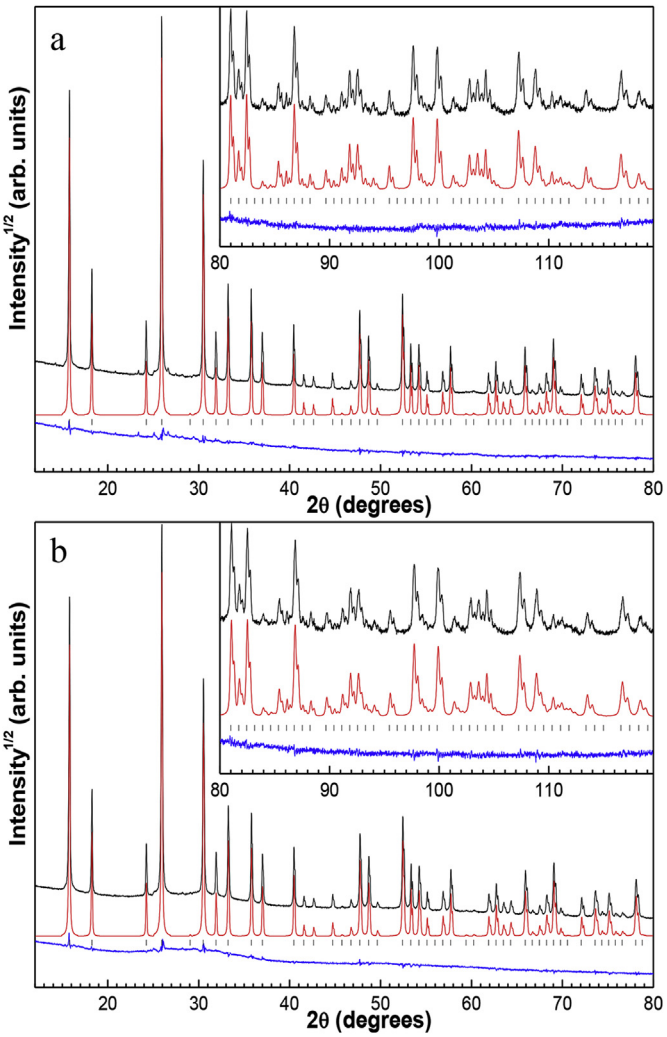

Fig. 8. Observed (top), calculated (mid), and difference (bottom) PXRD profiles after DDM crystal structure refinement of (a) analcime and (b) Zr-analcime.

Table 3
PXRD experimental details.

	Analcime	Zr-Analcime
Crystal data		
Chemical formula	$Na_{0.986}(Al_{0.986}Si_{2.014}O_6)(H_2O)_{0.977}$	$Na_{0.95}(Al_{0.95}Si_{2.05}O_6)(H_2O)_{0.946}$
Space group	*Ia-3d*	*Ia-3d*
Lattice parameter (Å)	13.7319 (4)	13.7219 (4)
V (Å^3)	2589.4 (2)	2583.7 (2)
Z	16	16
Temperature (K)	298	298
Radiation type	Cu Kα	Cu Kα
Refinement		
R factors and goodness of fit	$R_{DDM} = 0.056$, $R_{exp} = 0.021$, $R_{Bragg} = 0.018$, $R(F) = 0.020$, $\chi^2 = 2.646$	$R_{DDM} = 0.075$, $R_{exp} = 0.033$, $R_{Bragg} = 0.018$, $R(F) = 0.015$, $\chi^2 = 2.265$

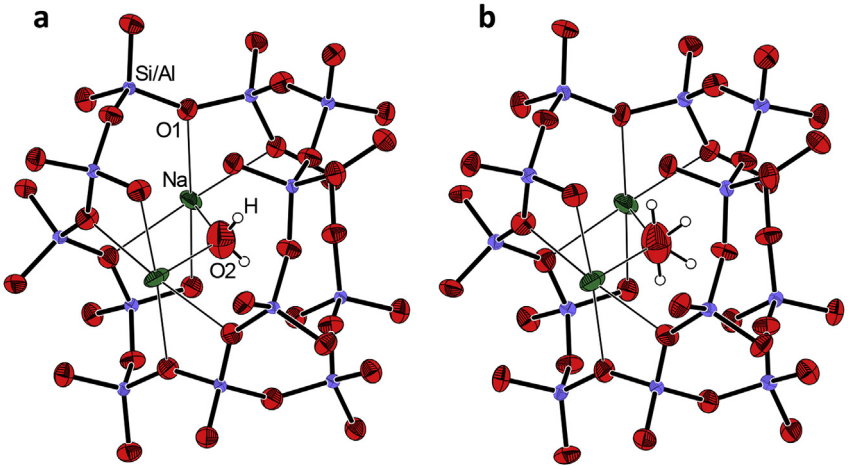

Fig. 9. Ellipsoid plot of analcime crystal structure determined from (a) PXRD and (b) single-crystal neutron diffraction [35].

displacement ellipsoids are perfectly reproduced for both refinements, emphasizing the accuracy of DDM. The ellipsoid plot shows that the water molecules are strongly disordered in the structure, which could be one of the reasons for the problematic location of H-positions in the neutron diffraction investigation [35]. In the DDM analysis, the displacement parameters of hydrogen atom were constrained with those of respective oxygen atom, which allowed a stable free refinement of H-coordinates without geometric restraints and gave reproducibly normal O-H distances as well as H-O-H and Na-O-H angles for both samples under investigation (Table 4).

The occupancies of Na and water sites were refined independently and the Si/Al ratio was determined from the resulted Na content in the structures giving the values of 2.04 and 2.16 for pristine analcime and Zr-analcime samples, respectively, which were close to those determined by the SEM-EDS (1.9 and 2.1). The revealed difference in the Si/Al ratios can be explained by different concentrations of sodium aluminate species in the reaction mixtures formed as a result of dissolution of CFAC aluminosilicate glass with participation of NaOH. In the case of the Zr involving synthesis, the zirconium salt added into the sodium alkaline solution is hydrolyzed resulting in $[ZrO_x(OH)_{4-2x}\cdot yH_2O]_n$ [39] and decreasing the concentration of active OH^- groups and, accordingly, $NaAlO_2$. The change of $NaAlO_2$ content in the alkaline solution of the lower NaOH concentration can be due also to kinetic factors of dissolution of CFAC glass which is inhomogeneous in chemical composition and contains regions enriched in Si, Al or other elements [40].

Table 4
Selected geometric parameters of analcime structure (Å, °).

Analcime			
Si—O1	1.6439 (5)	Na—O2	2.4275 (1)
Si—O1^{i}	1.6411 (5)	O2—H	0.85 (5)
Na—O1	2.5186 (5)		
O1—Si—O1^{ii}	105.20 (4)	O1—Na—O1^{v}	174.89 (2)
O1—Si—O1^{i}	111.20 (2)	O1—Na—O2	92.553 (11)
O1—Si—O1^{iii}	111.14 (3)	O1—Na—O2^{vi}	87.447 (11)
O1^{i}—Si—O1^{iii}	107.03 (4)	Na—O2—H^{vii}	105 (4)
O1—Na—O1^{ii}	62.46 (2)	Na—O2—H^{viii}	112 (4)
O1—Na—O1^{iv}	117.79 (2)	H—O2—H^{v}	102 (7)
Zr-Analcime			
Si—O1	1.6421 (4)	Na—O2	2.4257 (1)
Si—O1^{i}	1.6394 (4)	O2—H	0.86 (3)
Na—O1	2.5187 (4)		
O1—Si—O1^{ii}	105.30 (3)	O1—Na—O1^{v}	174.972 (17)
O1—Si—O1^{i}	111.160 (17)	O1—Na—O2	92.514 (8)
O1—Si—O1^{iii}	111.03 (2)	O1—Na—O2^{vi}	87.486 (8)
O1^{i}—Si—O1^{iii}	107.23 (3)	Na—O2—H^{vii}	113 (3)
O1—Na—O1^{ii}	62.434 (18)	Na—O2—H^{viii}	102 (3)
O1—Na—O1^{iv}	117.815 (18)	H—O2—H^{v}	105 (5)

Symmetry codes: (i) *z*-1/4, -*y*+1/4, -*x*+3/4; (ii) -*x*+1/4, *z*-1/4, *y*+1/4; (iii) -*z*+1/2, -*x*+1/2, -*y*+1/2; (iv) *x*, -*y*, -*z*+1/2; (v) -*x*+1/4, -*z*+1/4, -*y*+1/4; (vi) -*y*+1/4, *x*-1/4, *z*+1/4; (vii) *y*, *z*, *x*; (viii) *z*, *x*, *y*.

XRD peaks of ZrO_2 were not observed for the analcime-zirconia composite. A broad amorphous scattering between 20 and 40° 2Theta in Fig. 8b suggests that ZrO_2 is essentially amorphous in the sample.

Thus, as it is shown by the detailed PXRD analysis, the crystal structures and compositions of analcime resulted from both syntheses are close with a minor variation in the Si/Al ratio.

4. Conclusions

For the first time, analcime of a cubic structure with the Si/Al ratio of around 2.0 was synthesized as a single zeolite phase under hydrothermal conditions at 150 °C starting from CFAC with Si/Al = 2.7 as a Si and Al source. The microsphere particles with attached analcime crystals of 5–50 μm in size are the main product of the synthesis. In the presence of zirconium salt, analcime icositetrahedral crystallites with the Si/Al ratio of 2.16 and Zr content of 4.8 wt% are generated. Growth of identical Zr-analcime crystals with the narrow particle size distribution ($D_m = 41$ μm) takes place in the bulk of the reaction mixture and is likely to be controlled by the ratio of two parameters achieved under the reaction conditions, such as the release rate of silicate and aluminate species by dissolution of CFAC glass and the rate of crystal growth with participation of hydrolyzed Zr species which do not affect the zeolite topology but promote nucleation of zeolite. The crystal structures and compositions of analcime resulted from both syntheses are close with a minor variation in the Si/Al ratio. Zr atoms do not enter the zeolite structure as T-atoms or extra-framework cations but are the part of zirconia captured by the analcime crystals in the process of their growth. Refinement of complete crystal structures of the analcime samples using the DDM method provided detailed and reliable structural information from powder diffraction data including the anisotropic displacement parameters and positions of H-atoms.

The proposed sustainable approach to the synthesis of analcime based materials favours their application in different industrial fields, first of all, as sorbents of actinides and mineral-like matrices of ANA topology in ^{137}Cs nuclear waste disposal.

Acknowledgements

The work was supported by the State budget allocated to the fundamental research in the Russian Academy of Sciences in the framework of Project No. V.45.3.3. The authors acknowledge Dr. A. M. Zhizhaev for preparation and SEM-EDS examination of analcime polished cross-sections and Dr. Yu. L. Mikhlin for XPS measurement.

Appendix A. Supplementary data

Supplementary data related to this article can be found at https://doi.org/10.1016/j.micromeso.2017.09.011.

References

[1] D.W. Breck, Zeolite Molecular Sieves: Structure, Chemistry, and Use, John Wiley & Sons, New York, 1974.
[2] W.S. Wise, Handbook of Natural Zeolites, in: C. Colella (Ed.), International Zeolite Association, Natural Zeolites Commission, Napoli, Italy, 2013. A. De Frede Edotore : Natural Zeolites Commission.
[3] W.D. Balgord, R. Roy, Molecular Sieve Zeolites-1 Advances in Chemistry, 101, American Chemical Society, Washington, DC, 1971.
[4] S.H. Paek, C.D. Chung, G. Seo, Micropor. Mesopor. Mater. 155 (2012) 201–207.
[5] J.-N. Fang, I.-C. Lin, H.-J. Lo, S.-R. Song, Y.-L. Chen, J. Chin. Chem. Soc. 51 (2004) 1267–1272.
[6] Y. Wang, X. Li, Z. Xue, L. Dai, S. Xie, Q. Li, J. Phys. Chem. B 114 (2010) 5747–5754.
[7] B.S. Liu, C.T. Au, Chem. Lett. 31 (2002) 806–807.
[8] A. Bejar, S.B. Chaabene, M. Jaber, J.-F. Lambert, L. Bergaoui, Micropor. Mesopor. Mater. 196 (2014) 158–164.
[9] E.Z. Hegazy, I.H. Abd El Maksod, R.M.M. Abo El Enin, Appl. Clay Sci. 49 (2010) 149–155.
[10] N.G. Rachkova, A.I. Taskaev, Radiochemistry 53 (2011) 314–321.
[11] H. Mimura, M. Shibata, K. Akiba, J. Nucl. Sci. Technol. 27 (1990) 167–173.
[12] Z. Jing, K. Cai, Y. Li, J. Fan, Y. Zhang, J. Miao, Y. Chen, F. Jin, J. Nucl. Mater. 488 (2017) 63–69.
[13] J. Fan, Z. Jing, Y. Zhang, J. Miao, Y. Chen, F. Jin, Chem. Eng. J. 304 (2016) 344–350.
[14] A.F. Redkin, J.J. Hemley, Eur. J. Mineral. 12 (2000) 999–1014.
[15] M.A. Subramanian, D.R. Corbin, U. Chowdhry, Bul. Mat. Sci. 16 (1993) 665–678.
[16] A. Marocco, G. Dell'Agli, S. Esposito, M. Pansini, Solid State Sci. 14 (2012) 394–400.
[17] E.R. Begley, P.O. Herndon, Refract. Mater. 5 (1971) 185–208.
[18] I.W. Donald, Waste Immobilization in Glass and Ceramic Based Hosts: Radioactive, Toxic and Hazardous Wastes, John Wiley & Sons, Wiley-Blackwell Chichester, 2010.
[19] R.M. Barrer, Hydrothermal Chemistry of Zeolites, Academic Press, New York, 1982.
[20] (a) X. Querol, N. Moreno, J.C. Urnana, A. Alastuey, E. Hernandez, A. Lopez Soler, F. Plana, Int. J. Coal Geol. 50 (2002) 413–423;
(b) L. Zhou, Y.-L. Chen, X.-H. Zhang, F.-M. Tian, Z.-N. Zu, Mater. Lett. 119 (2014) 140–142.
[21] M.V. Sandoval, J.A. Henao, C.A. Rios, C.D. Williams, D.C. Apperley, Fuel 88 (2009) 272–281.
[22] D. Ma, Y. Shu, X. Han, X. Liu, Y. Xu, X. Bao, J. Phys. Chem. B 105 (2001) 1786–1793.
[23] A. Dyer, S. Tangkawanit, K. Rangsriwatananon, Micropor. Mesopor. Mater. 75 (2004) 273–279.
[24] T.A. Vereshchagina, S.N. Vereshchagin, N.N. Shishkina, L.A. Solovyov, N.G. Vasilieva, A.G. Anshits, J. Nucl. Mater. 437 (2013) 11–18.
[25] S.N. Vereshchagin, T.A. Vereshchagina, N.N. Shishkina, A.G. Anshits, Chem. Sustain. Devel 16 (2008) 511–519 (Transl. Khim. Interesakh Ustoich. Razvit.).
[26] T.A. Vereshchagina, S.N. Vereshchagin, N.N. Shishkina, L.A. Solovyov, O.A. Mikhaylova, A.G. Anshits, Micropor. Mesopor. Mater. 169 (2013) 207–211.
[27] N.N. Anshits, O.A. Mikhailova, A.N. Salanov, A.G. Anshits, Fuel 89 (2010) 1849–1862.
[28] E.V. Fomenko, N.N. Anshits, L.A. Solovyov, O.A. Mikhaylova, A.G. Anshits, Energy fuels 27 (2013) 5440–5448.
[29] E.V. Fomenko, N.N. Anshits, N.G. Vasil'eva, E.S. Rogovenko, O.A. Mikhaylova, E.V. Mazurova, L.A. Solovyev, A.G. Anshits, Solid Fuel Chem. 50 (2016) 238–247.
[30] Cements and materials for cement production, Chemical Analysis Methods, State Standard (GOST) No.5382-91, IPK Izdatel'stvo standartov, Moscow, 2002.
[31] H. Rietveld, J. Appl. Crystallogr. 2 (1969) 65–71.
[32] L.A. Solovyov, J. Appl. Crystallogr. 37 (2004) 743–749.
[33] P. Trens, M.J. Hudson, R. Denoyel, J. Mater. Chem. 8 (1998) 2147–2152.
[34] V. Pecharsky, P. Zavalij, Fundamentals of Powder Diffraction and Structural Characterization of Materials, second ed., Springer, US, 2009.
[35] G. Ferraris, D.W. Jones, J. Jerkess, Z. Krist. 135 (1972) 240–252.
[36] L.A. Solovyov, Acta Crystallogr. B72 (2016) 738–743.
[37] L.A. Solovyov, Acta Crystallogr. B68 (2012) 89–90.
[38] L.A. Solovyov, A.M. Astachov, M.S. Molokeev, A.D. Vasiliev, Acta Crystallogr. B61 (2005) 435–442.
[39] A. Clearfield, G.P.D. Serrette, A.H. Khazi-Syed, Catal. Today 20 (1994) 295–312.
[40] E.V. Fomenko, N.N. Anshits, N.G. Vasilieva, O.A. Mikhaylova, E.S. Rogovenko, A.M. Zhizhaev, A.G. Anshits, Energy fuels 29 (2015) 5390–5403.